Published in final edited form as:
Nat Struct Mol Biol. 2010 June ; 17(6): 768–774. doi:10.1038/nsmb.1807.

Structure determination of the seven-helical transmembrane receptor sensory rhodopsin II by solution NMR spectroscopy

Antoine Gautier, **Helen R. Mott**, **Mark J. Bostock**, **John P. Kirkpatrick**, and **Daniel Nietlispach***
Department of Biochemistry, University of Cambridge, 80 Tennis Court Road, Cambridge CB2 1GA, UK

Abstract

Seven-helical membrane proteins represent a challenge for structural biology. Here, we report the first NMR structure determination of a detergent-solubilized seven-helical transmembrane (7TM) protein, the phototaxis receptor sensory rhodopsin II (pSRII) from *Natronomonas pharaonis,* as a proof of principle. The overall quality of the structure ensemble is extremely good (backbone root mean squared deviation of 0.48 Å) and agrees well with previously determined X-ray structures. Furthermore, measurements in more native-like small phospholipid bicelles indicate that the protein structure is the same as in detergent micelles, suggesting that environment specific effects are minimal when using mild detergents. We use our case study as a platform to discuss the feasibility of similar solution NMR studies for other 7TM proteins including members of the family of G protein-coupled receptors (GPCRs).

Membrane proteins are highly abundant, comprising more than a third of all cellular proteins, but they are structurally under-represented (http://blanco.biomol.uci.edu/). To obtain high-resolution structural information on integral membrane proteins remains a great challenge. X-ray crystallography is the primary tool for structure determination but NMR spectroscopy has now established itself as a major technique for such proteins. While the polytopic α-helical membrane proteins in particular remain problematic targets for structure determination, encouraging contributions have recently emerged using X-ray crystallography1-3 and both solution4-8 and solid-state9-11 NMR spectroscopy. The structural inaccessibility of GPCRs has proved a particular bottleneck in understanding the mechanism of ligand binding and conformational changes associated with the activation of these proteins, which represent the largest family of receptors that signal across the eukaryotic cell membrane12. However, the past two years have seen some remarkable breakthroughs in the analysis of GPCR structures by X-ray crystallography13-16, as obstacles related to insufficient stability and conformational heterogeneity of GPCRs have been gradually circumvented2,3.

To date, only a few sizeable structures of α-helical membrane proteins have been solved by solution NMR4,17,18 of which only one is monomeric5. NMR spectroscopy is in principle

*to whom correspondence should be addressed: dn206@bioc.cam.ac.uk.

AUTHOR CONTRIBUTIONS
AG and JPK carried out protein expression, purification and detergent reconstitution. AG and HRM assigned resonances and carried out structure calculations. MJB did the spin label experiments and bicelle studies. DN wrote the manuscript and designed and conducted research including NMR data acquisition, processing, assignment of spectra, and data analysis.

Accession codes. RCSB PDB: Atomic coordinates of the structures of DHPC-micelle solubilized pSRII have been deposited under the PDB ID 2ksy. BioMagResBank: Chemical shifts have been deposited with entry number 16678.

COMPETING INTERESTS STATEMENT
The authors state that there are no conflicting interests.

Europe PMC Funders Author Manuscripts

able to report the structure and dynamics of such proteins and allows investigation of the very conformational mobility that to a large extent interferes with the process of crystallization. In particular, NMR techniques will be able to examine ligand-activated binding processes19 and will convey interactions with membrane-associated20 and other proteins within the membrane. Based on their size, many 350–400-residue detergent-reconstituted ligand-bound GPCRs should be amenable to investigation by solution NMR methodologies. However, so far comprehensive NMR studies of 7TM GPCR proteins in solution have been impaired by the substantial problems of sample preparation including the inability to produce sufficient quantities of isotopically labeled protein and the difficulties associated with the limited thermal stability, sample heterogeneity and the short lifetimes of such proteins.

Our study aimed to investigate the feasibility of determining the structure of a 7TM protein using solution based, state-of-the-art NMR methodologies. Since such a study is currently not feasible using GPCRs, we decided to focus on a 7TM protein that has many structural similarities to GPCRs whilst also displaying improved thermal stability and permitting expression in sufficient quantities to allow NMR investigations. In this work, we present the first three-dimensional structure of a seven-helical membrane protein receptor determined by NMR spectroscopy. We used pSRII21 from *Natronomonas pharaonis,* a 241-residue protein that can be expressed in sufficient quantities in *Escherichia coli* as a representative model protein for our structural investigations. pSRII functions via 13-*trans–cis* isomerization of its all-*trans* retinal group as a repellent phototactic receptor to blue light, enabling the archaeon to seek the dark when respiratory substrates are plentiful. Two crystal structures of ground-state pSRII have been solved previously22,23.

RESULTS

Detergent solubilization and sample optimization

To reduce the amount of protein required, we screened sample and detergent conditions in a micro-titer plate format. The stability of pSRII was assessed by monitoring the UV/vis absorbance at 498 nm characteristic of the bound retinal chromophore in the functional protein. Any conditions that led to a half-life of more than 12 hours were repeated on a larger scale for 1D and 2D ^{15}N NMR spectroscopy. For promising candidates, the size of the protein–detergent complex was then assessed by dynamic light scattering, size-exclusion chromatography and NMR translational diffusion measurements (data not shown).

Candidates with size estimates of the complex below 100 kDa were then further tested for their thermal stability. From a range of 20 systematically investigated sets of conditions, we selected the detergent diheptanoylphosphatidylcholine (DHPC) for solubilization of pSRII. The NMR spectral appearance improved continually with higher temperatures from 20 °C up to 50 °C and this detergent was found to balance acceptable spectral quality with sufficient sample stability at the elevated temperature employed for NMR spectroscopy24. Based on the rotational correlation time obtained from amide ^{15}N transverse cross-correlated cross relaxation rates and from translational diffusion coefficients, the size of the protein–detergent complex was estimated to be 70 kDa. This corresponds to monomeric pSRII protein that binds ~90 detergent molecules. Importantly, DHPC provided excellent sample homogeneity, resulting in NMR signal line widths that were in agreement with this estimate of the molecular weight of the complex (Supplementary Fig. 1 and Supplementary Table 1).

Backbone assignment and dynamics

We previously reported near-complete backbone assignments of pSRII24, based on six HN-detected transverse relaxation-optimized spectroscopy (TROSY) triple-resonance

experiments recorded on a highly deuterated sample. Reducing the sample pH by half a unit to pH 5.4 allowed us to complete the backbone assignment, revealing the final four residues that were undergoing intermediate exchange at the higher pH (Supplementary Fig. 2). Backbone assignments benefited from non-uniform sampling methods to increase the resolution and to a certain extent also the sensitivity24,25. Most experiments were recorded multiple times and after monitoring the sample integrity, the data sets were combined to increase the overall signal intensity. The improved sensitivity eventually resulted in a near-complete set of $^{13}C\alpha$ and $^{13}C\beta$ shift assignments. A total of 307 inter-amide distance restraints were observed in ^{15}N 3D nuclear Overhauser enhancement spectroscopy (NOESY) spectra using a highly deuterated sample. Water-exposed residues were located from amide–water exchange experiments that identified the loop regions and the solvent exposed flanks of the α-helices. ^{15}N spin relaxation data for the backbone indicated that there is limited flexibility in the shorter of the loop regions connecting the seven ordered helices of the transmembrane core, with more pronounced flexibility on the ps-ns timescale in the loops L1 and L2 connecting the first three α-helices and to some extent also in L5 24. The helical core of the protein is well structured and does not show any motion on this timescale.

To simulate the behavior of a slower-tumbling larger protein–detergent complex, we attempted to repeat the backbone assignment of pSRII at the lower temperature of 35 °C, while also increasing the concentration of DHPC from 3% to 10% (w/v). The increased solution viscosity under these conditions slows the tumbling of the protein–detergent complex, imitating the behavior of a 110 kDa complex at the lower temperature and higher detergent concentration. Despite the reduced spectral quality, we were still able to complete 90% of the sequential assignments as well as to obtain amide–amide NOEs.

Side chain assignment and structural restraints

As is typical for many membrane proteins, the hydrophobic residues Ile, Leu and Val in pSRII account for a substantial proportion of the sequence (32%), and furthermore, are distributed over all seven helices (Fig. 1a and Supplementary Fig. 3). Assignments for 140 out of 141 methyl groups in the Ile (δ1 only), Leu and Val residues were obtained using a highly deuterated, selectively methyl-protonated sample through methyl observation experiments26 (Fig. 1b and Supplementary Fig. 4). The ^{13}C spin systems of residues Val and Leu were linearized with only one of the methyl group positions (CH_3)–^{13}C labeled to maximize the sensitivity of the assignment experiments. Amide-based and methyl-detected experiments were used in a complementary fashion, with the latter being more sensitive as reported previously26.

The high level of methyl group assignment allowed the identification of a substantial number of NOE distances in ^{13}C-separated NOESY spectra (Fig. 1c). Exchange of the protein into micelles comprising the shorter side chain detergent dihexanoylphosphatidylcholine (c6-DHPC) resulted in a slight alteration of peak positions, providing the assignment of additional NOEs in situations of extreme peak overlap (Supplementary Fig. 5). Analysis of a 4D ^{13}C-separated NOESY spectrum also provided 30 long-range distance restraints between methyl groups located in different α-helices (Supplementary Fig. 6). The observation of methyl-to-amide NOEs in a ^{15}N-separated NOESY spectrum was also particularly useful (Supplementary Fig. 7). Although valuable for the definition of the overall architecture, structure calculations showed that these restraints were not sufficient to reliably define the relative orientation of the individual helices. Overall the data were not adequate to provide a reasonable global fold, indicating that additional structural restraints were required.

A limiting factor of the selective methyl-protonation labeling approach remained that many of the useful NOE signals were overlapped with or hidden by the strong diagonal signals in the spectra and so were not directly accessible. This situation could have been improved to some extent through the use of a sample with ^{13}C labels only in the methyl positions, which would have allowed acquisition of higher resolution NOESY spectra not limited by the scalar couplings between adjacent ^{13}C spins in uniformly labeled samples. Instead, further long-range NOEs were obtained by assigning the intense and well dispersed methyl groups of Ala, from a protonated sample, as well as the methyl groups of Thr, Met and Ile $\gamma 2$ (Supplementary Fig. 4 and Supplementary Table 2) using the same protonated sample. The inclusion of Ala assignments turned out to be highly complementary to the Ile, Leu and Val residues due to their positioning in those transmembrane regions where there was a lower density of Ile, Val and Leu side chains (the distribution of these residues is shown in Supplementary Fig. 3b).

Intra-helix methyl-methyl, methyl-HN and HN-HN NOEs, backbone chemical shift-derived dihedral angles and hydrogen bonds were sufficient to define the structure of the individual helices, but the quality of the structure, although improved, remained relatively low (backbone rmsd 3.0 Å, Supplementary Fig. 8). In particular, it was apparent when compared with the X-ray structures22,23 that although the individual helices were formed and their orientation was as anticipated, their overall packing lacked the necessary compaction, due to the absence of sufficient long-range distance restraints (Supplementary Fig. 8).

A model calculation using the X-ray structure coordinates of pSRII predicted 188 methyl–methyl distances of less than 5 Å but only 48 of these could be experimentally unambiguously observed in the NOESY spectra, leaving many peaks absent or too close to the diagonal to be assigned (Supplementary Table 2), such that the full NOE potential of the methyl-protonation approach could not be entirely exploited. Nevertheless, the near complete methyl group assignment of the Ile, Leu, Val, Ala, Thr and Met residues allowed us to complete the side chain assignment of the majority of these types of residues using a combination of deuterated and protonated samples (Fig. 1a and Supplementary Fig. 3b). The assignment of the complete side chains of the Ile, Leu, Val, Ala, Thr and Met residues, together with the short and medium-range distances observed in α-helices, permitted gradual expansion of the assignments to many adjacent residues as well as more distant residues within the individual α-helices (Fig. 1a). This iterative procedure, based mainly on the combined analysis of 3D HCCH COSY and ^{13}C- and ^{15}N-separated NOESY data improved the level of assignment across the protein, using the assigned methyl containing residues as starting points. Overall, this yielded an increased number of distance restraints per residue and the identification of more long-range inter-helix contacts (Supplementary Table 2). As expected for a protein of such a size whose tumbling is slowed by the presence of bound detergent, this approach was eventually limited by severe overlap in the ^{13}C-separated NOESY spectra and the effects of increased NMR line widths, precluding by far a complete resonance assignment. The quality of the spectra was further compromised by the presence of several very strong DHPC detergent signals, which masked vital spectral information even when efficient suppression methods were applied (deuterated DHPC is not commercially available) (Supplementary Figs. 4 and 9). Assignment of NOEs involving the aromatic side chains of Phe, Tyr and Trp residues was found to have a critical impact on the outcome of the structure calculations greatly helping to establish the inter-helix orientations in the protein core (Supplementary Table 2). The aromatic residues were assigned relying on 3D NOESY data.

The assignment of the side chains of the residues in the six loop regions followed a similar strategy, starting from the previously assigned methyl groups. The presence of a short section of anti-parallel β-sheet with a type II turn from residues 63 to 66 of the first

extracellular loop joining helices B and C was confirmed through its characteristic NOE pattern. The retinal moiety attached to Lys205 was assigned with the help of 2D *J*-correlation and NOESY spectroscopy, which also confirmed the all-*trans* conformation of the chromophore (Supplementary Table 3). Protein to retinal distance restraints were identified in ^{13}C-separated NOESY spectra and were confirmed as such by recording an equivalent ^{13}C-separated NOESY experiment without ^{13}C-decoupling in the indirect proton dimension.

Structure calculations

The 3D structure of pSRII was calculated using the program Aria27 interfaced to CNS28 on the basis of 5,564 distance restraints (4,055 unambiguous, 1,509 ambiguous), 190 pairs of backbone torsion angle restraints and 132 hydrogen bond restraints. The ambiguous distance restraints were handled using the ARIA methodology, where the ambiguity is resolved through iterative rounds of structure calculations. No prior knowledge based on crystal structure information was used when assigning long-range NOEs. The final structures are well defined, with a root mean squared deviation (rmsd) of 0.48 Å over the backbone residues 1–221 (Fig. 2a,b and NMR structure statistics Table 1). The remaining 20 residues of the C-terminal part of the protein are highly flexible and unstructured, as judged from relaxation experiments24 and did not display any long-range NOEs. The overall structure is in good agreement with the previously determined X-ray structures with a backbone rmsd of 1.23 Å between our structure and structure 1H6823 (Fig. 2c) and of 1.32 Å between the NMR structure and structure 1JGJ22 (the rmsd between the two X-ray structures is 0.37 Å). With a compact seven-helical core, the majority of the key structural features are in excellent accord and the overall orientation, packing and length of the helices match closely between the structures.

Protein-detergent interactions

The spin label reagents gadoteridol and 16-doxylstearicacid (16-DSA), which are water- and detergent-soluble, respectively, were used to establish the solvent-accessible extra-membrane residues and the hydrophobic surface that is contacted by the aliphatic detergent side chains29 (Fig. 3 and Supplementary Fig. 10). In both cases, proximity to the unpaired electron in the spin label led to a dramatic intensity reduction of all NMR signals of nearby protons (Fig. 3). While the loop regions and the helix termini were heavily broadened by the water-soluble gadoteridol, the effect of 16-DSA was maximal for outward pointing residues located in a band that wrapped around the center of the helices and that would be deeply buried in the membrane bilayer (Fig. 3a). As the region affected by relaxation enhancement formed a wide band across the hydrophobic region, a micellar prolate-monolayer ring model appeared to be the most likely mode of detergent binding. Interestingly, 16-DSA affected residues were biased towards the extracellular side, implying that pSRII may not be centered in the micelles, a conclusion supported by calculations of the hydrophobic core of pSRII30. Since pSRII is a light-driven receptor which signals into the cell, exposing more protein on the intracellular side of the membrane may promote interactions with the transducer, HtrII, facilitating signaling into the cytosol.

To further investigate the structural effects of DHPC solubilisation, and in particular possible detergent-micelle curvature-induced structural perturbations, pSRII was also reconstituted in more native-like small isotropic bicelles (DMPC/c6-DHPC ratio q=0.3). As a better mimic of the natural environment, small phospholipid bicelles have been used in the past to functionally reconstitute several membrane proteins31,32. The ^{15}N spectra of pSRII in small bicelles were generally broader, in agreement with their larger size, but chemical shift comparison with the DHPC spectra showed only minor differences, mostly affecting residues at the helix extremities (Fig. 4a, b and Supplementary Fig. 11). Similar ^{15}N-

NOESY patterns underlined that the protein showed only small and insignificant structural differences in the two environments (Fig. 4c).

DISCUSSION

Structure of sensory rhodopsin pSRII

We have solved the structure of sensory rhodopsin pSRII in DHPC micelles, the first structure of a 7TM protein determined by solution-NMR spectroscopy. The quality of the NMR structure obtained is excellent and the final set of structures is well defined showing the seven-helical core with the length of the α-helices matching those in the X-ray structures and with their packing and orientation also in close agreement. Aside from a few subtle differences, the resemblance between the X-ray and NMR structures of pSRII is striking (Fig. 2c). A closer analysis of the seven individual transmembrane helices in the superposition of the closest to the mean NMR structure with the X-ray structure 1H68 showed that rms deviations were small and varied between 0.66 Å for helix B to 1.02 Å for helix A (Supplementary Fig. 12). The side chain conformations are based predominantly on the use of unambiguous NOE assignments, of which a substantial number are available (Fig. 1a and Supplementary Fig. 3b). This has resulted in an average number of 15 NOEs per residue, of which 7 are short- or medium-range. The average pairwise rmsd over all the heavy atoms for residues 1–221 is 0.866 Å (Table 1). Loop L1 between helices A and B is in a slightly different position, but the ^{15}N relaxation data indicate increased mobility24 for this region. The chromophore position in the binding pocket is well defined and shows a similar arrangement to those in the X-ray structures (Fig. 2d). The NMR structure shows several distinct features of the retinal binding pocket where Asp75 and Asp201, which act as counter ions to the protonated Schiff base, are pointing in its direction and are located in similar positions to the X-ray structures, indicating that the separation of these residues to the counter ion is maintained when pSRII is solubilized in DHPC. One of the residues that has been postulated to contribute to the blue-shifted colour-tuning of the rhodopsin, Arg72, is tilted away from the Schiff base and points towards the extracellular side, as observed in the X-ray crystal structures22,23. All these observations endorse the reliability of the determined side chain conformations. No major structural differences were apparent when comparing detergent-micelle and small bicelle environments, endorsing the validity of studies performed in mild detergents.

The choice of our structure determination strategy was conservative and relied primarily on NOE distance information, supplemented by dihedral angles and hydrogen bonds in the α-helical regions. The complementary use of a mixture of deuterated, selectively protonated and fully protonated samples substantially increased the number of interpretable NOEs and resulted in a high quality structure. The process was facilitated by the initial successful assignment of many methyl groups, which allowed the propagation of assignments onto other protons within those residues. Subsequently, we were able to assign residues that were in close proximity to the methyl-containing residues, thereby leading to a markedly increased number of medium- and long-range distances and dramatically improving the quality of the structure. The primary aim of this work was to use pSRII as a model system for testing the feasibility of a NMR structure determination of a 7TM protein. Having solved the structure of pSRII, the question remains as to how representative or transferable this approach might be to other, potentially more sizeable proteins, such as the large family of G protein-coupled receptors and how successful following a similar strategy would be in solving their structures. In what follows, we discuss the possibilities and limitations and describe conditions we feel are likely to be necessary for such structure determinations to be successful.

Europe PMC Funders Author Manuscripts

Perspectives for GPCR proteins

Studies of GPCRs are currently challenging for any structural technique as these proteins express in small quantities and are of limited stability, particularly in their unbound state. Samples must be conformationally and chemically homogeneous and stable at high concentrations. Compared to other structural methods, current NMR studies of GPCRs are impeded by the additional requirement for isotopically labeled samples. Despite these problems there are encouraging indications suggesting that in the near future, heterologous expression systems will provide labeled GPCRs in sufficient quantities to produce NMR samples. Certain GPCRs can already be expressed in *E.coli* in functional form33-38. The levels of expressed protein are relatively small, requiring large-scale preparations, which for isotopically labeled samples are necessarily rather expensive. The recent successful refolding of several GPCRs39 has shown that the high level production of GPCRs from *E. coli* inclusion bodies presents a viable choice for obtaining such proteins40. Alternative systems to *E.coli* that allow the expression of isotopically labeled proteins are becoming available for GPCRs41,42, such as *P. pastoris43*, cell-free based expression systems44 and baculovirus–insect cells45.

Undoubtedly pSRII combines several favourable characteristics that helped to improve the quality of the final structures. Any forecasts based on pSRII need to be qualified by considering how much of a non-universally applicable advantage these properties may have represented.

While the improvements from the carefully optimized pSRII sample conditions together with the excellent spectral dispersion were of great benefit for the ^{15}N-based backbone assignment task, their favourable impact was far less noticeable with regard to the ^{13}C spectra. In general the latter spectra were very crowded. Aromatic residues typically increase the signal dispersion but in pSRII the number of these residues is slightly below the average expected for the transmembrane regions of such proteins46. On the other hand, the distribution of methyl-containing residues in pSRII is very typical for α-helical membrane proteins. A similar assignment strategy for the methyl-containing residues should therefore be equally applicable to other 7TM proteins.

The majority of membrane protein NMR studies to date have been conducted at elevated temperatures of 35–45 °C6 including our work at 50 °C. It is unrealistic to propose high temperature studies using wild-type GPCRs. Even at room temperature, their lifetimes may be too limited to allow the recording of 3D spectra. Nevertheless, progress has recently been made through limited mutagenesis leading to the production of substantially thermostabilized GPCRs, as was shown for β_1-AR15, bovine rhodopsin47 and the A_{2a} receptor48. Since NMR spectroscopy benefits from the effects of the increased spin-state lifetimes at higher temperatures, suitable GPCRs will need to be sufficiently thermally stabilized. Such stabilization has been used to great benefit for recent X-ray structure determinations and is certain to become a general and determining necessity for undertaking NMR studies. We have obtained preliminary 1D NMR and translational diffusion results on a *bona fide* GPCR, a 320-residue β_1-adrenergic receptor that has been thermostabilized through such limited mutagenesis15 (Supplementary Table 4). Our preliminary results reveal a sample lifetime at 35 °C of 5 days, which is of sufficient length to record complex heteronuclear NMR experiments once an isotopically labeled sample becomes available. The size of the solubilized protein was found to be only ~25% larger (~85 kDa) than pSRII, which from a sensitivity perspective is well within the functioning limits of the methods described here. The feasibility of working on a larger protein–detergent complex was also simulated by repeating the backbone assignment of pSRII at a lower temperature of 35 °C and higher detergent concentration, under which conditions the increased solution viscosity imitated the behavior of a larger 110 kDa sized complex. Even under these conditions we

were able to complete 90% of the sequential assignments as well as obtaining numerous amide–amide NOEs.

Increased spectral overlap for larger proteins will require the adaptation of the NMR approach to prevent a deterioration of the achievable structure quality due to a lack of NOEs. In our experience, it was relatively easy to build the individual helices based on NOEs, dihedral angles and hydrogen bond restraints. This information is likely to still be available for a protein larger than pSRII, so that we expect the delineation of the α-helices to remain feasible. GPCRs vary substantially in size but this should still work for the small-to-medium sized (350–400 residues) members of this extensive protein family. Alternative methods can then be used to determine the orientation and packing of the α-helices in order to compensate for the probable lack of interpretable long-range NOEs. The efficient use of such complementary structural information in the form of paramagnetic relaxation enhancement techniques (PRE)49 has been successfully demonstrated for membrane proteins using site-directed spin labeling5,50. If required, this powerful distance method can be further supplemented by techniques that rely on the introduction of a small level of anisotropy to exploit pseudo-contact shifts (PCSs)51,52 and dipolar couplings (RDCs)53-55 to further improve the relative orientation of the individual helices. Such approaches will remain suitable for proteins larger than pSRII, for which overlap of the side chain signals has become too extensive to allow substantial assignment of long-range information.

In summary, we have shown by our high-quality structure of the archaeal protein receptor pSRII that the structure elucidation of a detergent-solubilized 7TM protein is feasible by high-resolution NMR. Based on these results, following a careful review of the impact various influential factors have on the progress of such studies and after evaluating in particular also if the more beneficial properties of pSRII might have overly aided our work, we come to the conclusion that similar NMR methods should be applicable to small-to-medium sized members of the important GPCR family of 7TM proteins, even if their larger size compared with pSRII will require certain modification to the strategy employed for pSRII. The NMR techniques to undertake such structural studies are available today. Such work will require substantial quantities of isotopically labeled GPCRs, and while this is still a challenge to obtain, recent work has made appreciable progress towards overcoming the current obstacles. It will be necessary to conduct structural studies at elevated temperatures, requiring the use of engineered GPCRs, where mutations have appreciably increased the thermal stability and lifetime of the proteins. Such engineering methods have recently been established and have resulted in the successful solution of several X-ray crystal structures. These techniques can be readily transferred to other proteins, which will lead to sufficiently stabilized GPCRs for solution NMR studies. Overall, the outlook is very encouraging and, together with the results presented here, indicates that many smaller GPCRs should soon be accessible to structural studies using solution NMR techniques.

Supplementary Material

Refer to Web version on PubMed Central for supplementary material.

Acknowledgments

This work was supported by a grant from the Royal Society (RG 2005/R1 and BBSRC (BB/G011915/1). A.G. was supported by a Marie Curie Actions studentship sponsored by the European Union. We thank Y. Ito (TMU, Japan) for discussions and assistance with NMR experiments and D. Moskau and R. Kuemmerle (Bruker Biospin, Faellanden) who helped with NMR measurements. We thank T.Warne for the preparation of β_1-AR. The use of the CamGrid computing resource is acknowledged for the structure calculations. The NMR Facility of the Department of Biochemistry is supported by the BBSRC, CRUK and the Wellcome Trust. We thank E.D. Laue and C.-W. Chung for their support in the initial stages of the project.

Appendix

METHODS

Sample preparation

For the expression of pSRII(1-241)21 the psopII gene from *Natronomonas pharaonis* plus a sequence encoding a C-terminal $(His)_6$-tag was inserted into the pET-28b(+) vector and transformed into the *E. coli* expression strain BL21 Tuner (DE3) (the original plasmid was obtained as a gift from J. Navarro, UTMB, Galveston, USA). Cells were grown in M9 minimal medium at 37 °C and expression was induced at an OD_{600nm} of 1.0 by the addition of 1 mM IPTG. At the same time, 10 μM all-*trans*-retinal was added. After 8 h the cells were resuspended and lysed using an Emulsiflex (Avestin, Inc.). Crude membranes were collected by ultracentrifugation (100,000 g for 90 min at 4 °C) and resuspended in 1/40th of the original culture volume using 50 mM MES-NaOH pH 6.5, 300 mM NaCl. The detergent dodecyl-β-D-maltoside (DDM) was added to a final concentration of 1.5% (w/v) and the mixture was incubated overnight. Insoluble material was removed by ultracentrifugation (100,000 g, 1 h, 4 °C). Solubilized pSRII was purified with Ni-NTA affinity beads (Novagen) in 50 mM MES-NaOH. The beads were washed with 30 column volumes of the same buffer containing 0.06% DDM. The protein was eluted in 50 mM TRIS-HCl pH 7.0, 300 mM NaCl, 0.1% DDM containing 150 mM imidazole and the solution exchanged into phosphate buffer by repeated rounds of concentration and dilution with a final volume of 0.5 ml. For the preparation of NMR samples, the protein was mixed with Ni-NTA beads as before and after removal of the flow-through, washed with 50 column volumes 20 mM sodium phosphate buffer pH 7.0, 50 mM NaCl containing 0.6% DHPC (1,2-diheptanoyl-sn-glycero-3-phosphocholine). The protein was eluted in the same buffer containing 300 mM imidazole and the eluted solution repeatedly concentrated and diluted in a concentrator (10 kDa cut-off) with 60 ml sodium phosphate pH 5.9, 50 mM NaCl containing 0.06% (w/v) DHPC to a final volume of 0.45 ml.

Isotope labelled samples

^{13}C and/or ^{15}N isotope labelled samples were produced from M9 medium containing 4 g l^{-1} ^{13}C-glucose and 1 g l^{-1} $^{15}NH_4Cl$. Highly deuterated protein was expressed following sub-culturing of the freshly transformed cells in M9 minimal medium with progressively higher D_2O content (50 %, 70 %, 90 %, 100 %). *U*-[^{2}H,^{13}C]-glucose was used as the sole carbon source and expression conditions were similar to the ones described above. Selectively methyl protonated samples were obtained by supplementation with 50 mgl^{-1} of α-ketobutyric acid (Cambridge Isotope laboratories) and 80 mgl^{-1} α-ketovaleric acid (Isotec) one hour before induction56. The following samples were prepared: Two samples of *U*-[^{2}H,^{15}N]-pSRII, four of *U*-[^{15}N]-pSRII, one of *U*-[^{13}C,^{15}N]-pSRII, two *U*-[^{2}H,^{13}C,^{15}N]-pSRII and two of *U*-[^{2}H,^{13}C,^{15}N] Ile δ1-[$^{13}CH_3$] Leu,Val-[$^{13}CH_3$,^{12} CD_3]-pSRII. Typical protein concentrations were 0.4-0.5 mM as determined from UV_{280} and UV_{498}. All samples were solubilized in DHPC (ca. 120x excess). DHPC was purchased from Avanti Polar Lipids, Inc., Birmingham, AL, USA. DHPC is not commercially available in deuterated form. All isotope labels were bought from Isotec, USA, except for α-ketobutyric acid which was obtained from Cambridge Isotopes, Andover MA, USA.

NMR spectroscopy

NMR experiments were recorded at 50 °C on Bruker DRX800 and DRX600 spectrometers equipped with cryogenic and conventional TXI probes. The following experiments were recorded57: 2D NOESY, 2D DQF COSY, 2D [^{1}H,^{15}N]-TROSY, 2D ^{13}C-HSQC, 2D ^{13}C-HMQC, 2D ^{13}C-CT-HSQC, 2D ^{13}C-CT-HMQC. 3D NUS25 recorded versions of the TROSY experiments HNCA, HN(CO)CA, HNCA(CO), HNCO, HN(CA)CB,

HN(COCA)CB. 3D NOESY ^{15}N-HMQC, 3D NOESY ^{15}N-HSQC, 3D NOESY-[^{1}H,^{15}N]-TROSY, 4D HNNH HMQC-NOESY-HMQC. 3D Val-(HM)CM(CBCA)NH, 3D Leu-(HM)CM(CGCBCA)NH, 3D Ile-(HM)CM(CGCBCA)NH, 3D Leu-HM(CMCBCBCA)NH, 3D Ala-HMCA, 3D HMCM(CG)CBCA, 3D (H)CCH COSY, 3D H(C)CH COSY, 3D NOESY ^{13}C-HSQC, 3D NOESY ^{13}C-HMQC, 4D HCCH HMQC-NOESY-HMQC, CT$\eta_{xy\text{-}IP/AP}$-[^{1}H,^{15}N]-TROSY, [^{1}H,^{15}N]-TRACT, BPP-LED.

Structure determination

Structures were calculated using CNS1.028 and Aria1.227 where the ambiguity of the NOEs is decreased in an iterative manner. Backbone torsion angle restraints were determined from chemical shift data using TALOS58. The retinal was modeled in a fixed double-bond trans arrangement and covalently bonded to the Nε of Lys205. NOE cross-peaks were observed between pSRII and the retinal, which was sufficient to define the binding pocket. Structures were calculated by 180 ps of torsion angle dynamics, followed by 72 ps of slow cooling in torsion angle space and 72 ps of slow cooling in Cartesian space. In the final iteration 100 structures were calculated, of which the 30 with the lowest energy were selected for further analysis. These structures had no NOE violations greater than 0.5 Å and no dihedral angle violations greater than 6°. Ramachandran plot statistics are as follows: most favoured (93.9%), additionally allowed (5.3%), generously allowed (0.2%) and disallowed (0.6%).

Titration with spin label

PRE experiments were performed as titrations by stepwise addition of the spin label reagent to 500 μl ^{15}N-labelled pSRII, using detergent-soluble 16-doxylstearic acid (16-DSA) (2-(14-carboxytetradecyl)-2-ethyl-4,4-dimethyl-3-oxazolidinyloxy, free radical; Sigma-Aldrich) in the range 0–16 mM and water-soluble gadoteridol (gadolinium complex of 10-(2-hydroxy-propyl)-1,4,7,10-tetraazacyclododecane-1,4,7-triacetic acid; trade-name Prohance, Bracco Diagnostics) in the range 0–50 mM. 16-DSA powder was dissolved in methanol and gadoteridol dissolved in water and aliquots prepared (16-DSA: 0.5, 1, 2, 3, 8, 16 mM and gadoteridol: 0.25, 0.5, 1, 2, 5, 10, 15, 30, 50 mM). Methanol was evaporated in a SpeedVac, to ensure no solvent-induced chemical-shift changes occurred. pSRII was then added to a given aliquot and the solution sonicated in a water bath (15 min) ensuring that 16-DSA was incorporated into the DHPC vesicles. Volume changes were taken into account in the analysis. 2D [^{1}H,^{15}N]-TROSY and 1D ^{1}H NMR spectra were recorded at 50 °C prior to the addition of spin label reagents, as reference spectra, and for each concentration.

Small isotropic bicelles

All NMR experiments of pSRII solubilized in small isotropic bicelles ([DMPC]/[c6-DHPC] q=0.3) were recorded at 40 °C. For comparison, spectra of pSRII in DHPC were also recorded at 40 °C and ^{1}H,^{15}N assignments were transferred.

REFERENCES

1. Tate CG, Schertler GFX. Engineering G protein-coupled receptors to facilitate their structure determination. Curr. Opin. Struct. Biol. 2009; 19:386–95. [PubMed: 19682887]
2. Topiol S, Sabio M. X-ray structure breakthroughs in the GPCR transmembrane region. Biochem. Pharmacol. 2009; 78:11–20. [PubMed: 19447219]
3. Weis WI, Kobilka BK. Structural insights into G protein-coupled receptor activation. Curr. Opin. Struct. Biol. 2008; 18:734–740. [PubMed: 18957321]
4. Van Horn WD, et al. Solution Nuclear Magnetic Resonance Structure of Membrane-Integral Diacylglycerol Kinase. Science. 2009; 324:1726–1729. [PubMed: 19556511]
5. Zhou YP, et al. NMR solution structure of the integral membrane enzyme DsbB: Functional insights into DsbB-catalyzed disulfide bond formation. Mol. Cell. 2008; 31:896–908. [PubMed: 18922471]

6. Kim HJ, Howell SC, Van Horn WD, Jeon YH, Sanders CR. Recent advances in the application of solution NMR spectroscopy to multi-span integral membrane proteins. Prog. Nucl. Magn. Reson. Spectrosc. 2009; 55:335–360. [PubMed: 20161395]
7. Tamm LK, Liang BY. NMR of membrane proteins in solution. Prog. Nucl. Magn. Reson. Spectrosc. 2006; 48:201–210.
8. Sanders CR, Sonnichsen F. Solution NMR of membrane proteins: practice and challenges. Magn. Reson. Chem. 2006; 44:S24–S40. [PubMed: 16826539]
9. Li Y, Berthold DA, Gennis RB, Rienstra CM. Chemical shift assignment of the transmembrane helices of DsbB, a 20-kDa integral membrane enzyme, by 3D magic-angle spinning NMR spectroscopy. Protein Sci. 2008; 17:199–204. [PubMed: 18227427]
10. Hong M. Structure, topology, and dynamics of membrane peptides and proteins from solid-state NMR Spectroscopy. J. Phys. Chem. B. 2007; 111:10340–10351. [PubMed: 17685648]
11. McDermott A. Structure and Dynamics of Membrane Proteins by Magic Angle Spinning Solid-State NMR. Ann. Rev. Biophys. 2009; 38:385–403. [PubMed: 19245337]
12. Loll PJ. Membrane protein structural biology: the high throughput challenge. J. Struct. Biol. 2003; 142:144–153. [PubMed: 12718926]
13. Jaakola VP, et al. The 2.6 Angstrom Crystal Structure of a Human A2A Adenosine Receptor Bound to an Antagonist. Science. 2008; 322:1211–1217. [PubMed: 18832607]
14. Scheerer P, et al. Crystal structure of opsin in its G-protein-interacting conformation. Nature. 2008; 455:497–502. [PubMed: 18818650]
15. Warne T, et al. Structure of a beta1-adrenergic G protein-coupled receptor. Nature. 2008; 454:486–491. [PubMed: 18594507]
16. Rasmussen SGF, et al. Crystal structure of the human beta2 adrenergic G protein-coupled receptor. Nature. 2007; 450:383–387. [PubMed: 17952055]
17. Oxenoid K, Chou JJ. The structure of phospholamban pentamer reveals a channel-like architecture in membranes. Proc. Natl. Acad. Sci. USA. 2005; 102:10870–10875. [PubMed: 16043693]
18. Schnell JR, Chou JJ. Structure and mechanism of the M2 proton channel of influenza A virus. Nature. 2008; 451:591–595. [PubMed: 18235503]
19. Bokoch MP, et al. Ligand-specific regulation of the extracellular surface of a G-protein-coupled receptor. Nature. 2010; 463:108–112. [PubMed: 20054398]
20. Ridge KD, et al. Conformational changes associated with receptor-stimulated guanine nucleotide exchange in a heterotrimeric G-protein alpha-subunit - NMR analysis of GTP gamma S-bound states. J. Biol. Chem. 2006; 281:7635–7648. [PubMed: 16407225]
21. Shimono K, Iwamoto M, Sumi M, Kamo N. Functional expression of pharaonis phoborhodopsin in Escherichia coli. FEBS Lett. 1997; 420:54–56. [PubMed: 9450549]
22. Luecke H, Schobert B, Lanyi JK, Spudich EN, Spudich JL. Crystal structure of sensory rhodopsin II at 2.4 angstroms: Insights into color tuning and transducer interaction. Science. 2001; 293:1499–1503. [PubMed: 11452084]
23. Royant A, et al. X-ray structure of sensory rhodopsin II at 2.1-angstrom resolution. Proc. Natl. Acad. Sci. USA. 2001; 98:10131–10136. [PubMed: 11504917]
24. Gautier A, Kirkpatrick JP, Nietlispach D. Solution-state NMR spectroscopy of a seven-helix transmembrane protein receptor: Backbone assignment, secondary structure, and dynamics. Angew. Chem. 2008; 47:7297–7300. [PubMed: 18677733]
25. Rovnyak D, et al. Accelerated acquisition of high resolution triple-resonance spectra using non-uniform sampling and maximum entropy reconstruction. J. Magn. Reson. 2004; 170:15–21. [PubMed: 15324754]
26. Tugarinov V, Kay LE. Ile, Leu, and Val methyl assignments of the 723-residue malate synthase G using a new labeling strategy and novel NMR methods. J. Am. Chem. Soc. 2003; 125:13868–13878. [PubMed: 14599227]
27. Linge JP, Habeck M, Rieping W, Nilges M. ARIA: automated NOE assignment and NMR structure calculation. Bioinformatics. 2003; 19:315–316. [PubMed: 12538267]
28. Brunger AT, et al. Crystallography & NMR system: A new software suite for macromolecular structure determination. Acta Crystallogr. D. 1998; 54:905–921. [PubMed: 9757107]

29. Hilty C, Wider G, Fernandez C, Wuthrich K. Membrane protein-lipid interactions in mixed micelles studied by NMR spectroscopy with the use of paramagnetic reagents. Chembiochem. 2004; 5:467–473. [PubMed: 15185370]
30. Gordeliy VI, et al. Molecular basis of transmembrane signalling by sensory rhodopsin II-transducer complex. Nature. 2002; 419:484–487. [PubMed: 12368857]
31. Poget SF, Cahill SM, Girvin ME. Isotropic bicelles stabilize the functional form of a small multidrug-resistance pump for NMR structural studies. J. Am. Chem. Soc. 2007; 129:2432–2433. [PubMed: 17284035]
32. Czerski L, Sanders CR. Functionality of a membrane protein in bicelles. Anal. Biochem. 2000; 284:327–333. [PubMed: 10964416]
33. Bertin B, et al. Functional Expression of the Human Serotonin 5-Ht1a Receptor in Escherichia-Coli - Ligand-Binding Properties and Interaction with Recombinant G-Protein Alpha-Subunits. J. Biol. Chem. 1992; 267:8200–8206. [PubMed: 1533220]
34. Furukawa H, Haga T. Expression of functional M-2 muscarinic acetylcholine receptor in Escherichia coli. J. Biochem. 2000; 127:151–161. [PubMed: 10731678]
35. Grisshammer R, Little J, Aharony D. Expression of Rat Nk-2 (Neurokinin-a) Receptor in Escherichia-Coli. Recept. Channels. 1994; 2:295–302. [PubMed: 7719707]
36. Hampe W, et al. Engineering of a proteolytically stable human beta(2)-adrenergic receptor/maltose-binding protein fusion and production of the chimeric protein in Escherichia coli and baculovirus-infected insect cells. J. Biotechnol. 2000; 77:219–234. [PubMed: 10682281]
37. Serrano-Vega MJ, Magnani F, Shibata Y, Tate CG. Conformational thermostabilization of the beta 1-adrenergic receptor in a detergent-resistant form. Proc. Natl. Acad. Sci. USA. 2008; 105:877–882. [PubMed: 18192400]
38. Weiss HM, Grisshammer R. Purification and characterization of the human adenosine A(2a) receptor functionally expressed in Escherichia coli. Eur. J. Biochem. 2002; 269:82–92. [PubMed: 11784301]
39. Dahmane T, Damian M, Mary S, Popot JL, Baneres JL. Amphipol-Assisted in Vitro Folding of G Protein-Coupled Receptors. Biochemistry. 2009; 48:6516–6521. [PubMed: 19534448]
40. Michalke K, et al. Mammalian G-protein-coupled receptor expression in Escherichia coli: I. High-throughput large-scale production as inclusion bodies. Anal. Biochem. 2009; 386:147–155. [PubMed: 19150325]
41. Junge F, et al. Large-scale production of functional membrane proteins. Cell. Mol. Life Sci. 2008; 65:1729–1755. [PubMed: 18408885]
42. McCusker EC, Bane SE, O'Malley MA, Robinson AS. Heterologous GPCR expression: A bottleneck to obtaining crystal structures. Biotechnol. Prog. 2007; 23:540–547. [PubMed: 17397185]
43. Andre N, et al. Enhancing functional production of G protein-coupled receptors in Pichia pastoris to levels required for structural studies via a single expression screen. Protein Sci. 2006; 15:1115–1126. [PubMed: 16597836]
44. Ishihara G, et al. Expression of G protein coupled receptors in a cell-free translational system using detergents and thioredoxin-fusion vectors. Protein Expr. Purif. 2005; 41:27–37. [PubMed: 15802218]
45. Akermoun M, et al. Characterization of 16 human G protein-coupled receptors expressed in baculovirus-infected insect cells. Protein Expr. Purif. 2005; 44:65–74. [PubMed: 15951199]
46. Liu Y, Engelman DM, Gerstein M. Genomic analysis of membrane protein families: abundance and conserved motifs. Genome Biol. 2002; 3 research0054.
47. Standfuss J, et al. Crystal structure of a thermally stable rhodopsin mutant. J. Mol. Biol. 2007; 372:1179–1188. [PubMed: 17825322]
48. Magnani F, Shibata Y, Serrano-Vega MJ, Tate CG. Co-evolving stability and conformational homogeneity of the human adenosine A(2a) receptor. Proc. Natl. Acad. Sci. USA. 2008; 105:10744–10749. [PubMed: 18664584]
49. Battiste JL, Wagner G. Utilization of site-directed spin labeling and high-resolution heteronuclear nuclear magnetic resonance for global fold determination of large proteins with limited nuclear overhauser effect data. Biochemistry. 2000; 39:5355–5365. [PubMed: 10820006]

50. Liang BY, Bushweller JH, Tamm LK. Site-directed parallel spin-labeling and paramagnetic relaxation enhancement in structure determination of membrane proteins by solution NMR spectroscopy. J. Am. Chem. Soc. 2006; 128:4389–4397. [PubMed: 16569016]
51. Bertini I, Luchinat C, Parigi G. Paramagnetic constraints: An aid for quick solution structure determination of paramagnetic metalloproteins. Concept Magnetic Res. 2002; 14:259–286.
52. Haussinger D, Huang JR, Grzesiek S. DOTA-M8: An Extremely Rigid, High-Affinity Lanthanide Chelating Tag for PCS NMR Spectroscopy. J. Am. Chem. Soc. 2009; 131:14761–14767. [PubMed: 19785413]
53. Cierpicki T, Liang BY, Tamm LK, Bushweller JH. Increasing the accuracy of solution NMR structures of membrane proteins by application of residual dipolar couplings. High-resolution structure of outer membrane protein A. J. Am. Chem. Soc. 2006; 128:6947–6951. [PubMed: 16719475]
54. Kamen DE, Cahill SM, Girvin ME. Multiple alignment of membrane proteins for measuring residual dipolar couplings using lanthanide ions bound to a small metal chelator. J. Am. Chem. Soc. 2007; 129:1846–1847. [PubMed: 17253688]
55. Tjandra N, Bax A. Direct measurement of distances and angles in biomolecules by NMR in a dilute liquid crystalline medium. Science. 1997; 278:1111–1114. [PubMed: 9353189]
56. Goto NK, Gardner KH, Mueller GA, Willis RC, Kay LE. A robust and cost-effective method for the production of Val, Leu, Ile (d1) methyl-protonated N-15-, C-13-, H-2-labeled proteins. J. Biomol. NMR. 1999; 13:369–374. [PubMed: 10383198]
57. Sattler M, Schleucher J, Griesinger C. Heteronuclear multidimensional NMR experiments for the structure determination of proteins in solution employing pulsed field gradients. Prog. Nucl. Magn. Reson. Spectrosc. 1999; 34:93–158.
58. Cornilescu G, Delaglio F, Bax A. Protein backbone angle restraints from searching a database for chemical shift and sequence homology. J. Biomol. NMR. 1999; 13:289–302. [PubMed: 10212987]

Europe PMC Funders Author Manuscripts

Europe PMC Funders Author Manuscripts

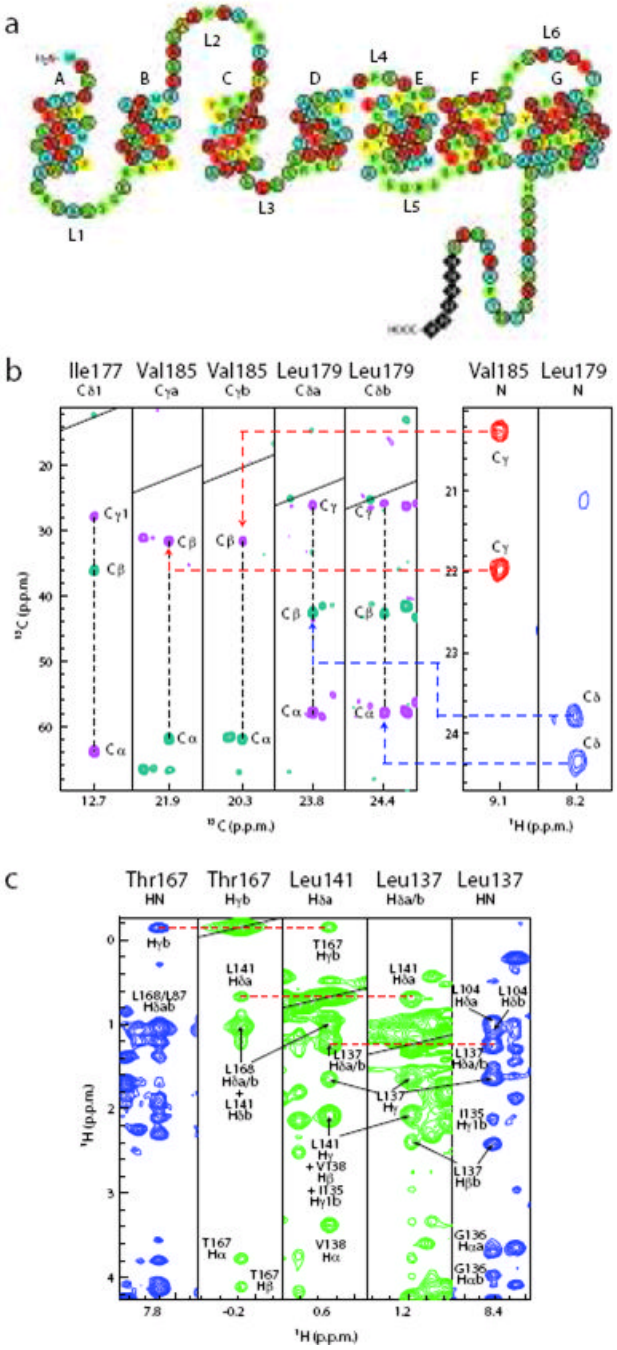

Figure 1.

Side chain assignment and NOE-derived distance restraints in pSRII. **(a)** Extent of the side chain assignments mapped onto a schematic topology cartoon of pSRII displaying the α-helices A–G and loops L1–L6. Residue types are color coded as Ile, Leu, Val in red, Ala, Met, Thr in blue, Phe, Trp, Tyr in yellow and all remaining residues in green. Residues with full proton assignments are encircled in bold while no circles indicate only partial side chain assignments. **(b)** A combination of ^{13}C-^{13}C cross-sections at the methyl ^{1}H frequencies of representative Ile, Leu and Val residues from methyl-separated experiments (left) and ^{1}H-^{13}C strip plots of the same residues at the corresponding backbone ^{15}N frequencies

(right) from 3D *J*-assignment experiments shows the correlation of backbone signals with the methyl resonances. **(c)** ^{1}H-^{1}H cross-sections from 3D ^{15}N- or ^{13}C-separated NOESY-HSQC spectra at the ^{15}N (blue) or ^{13}C (green) frequencies of selected residues. Intra- and inter-residue NOEs are indicated with annotations.

Europe PMC Funders Author Manuscripts

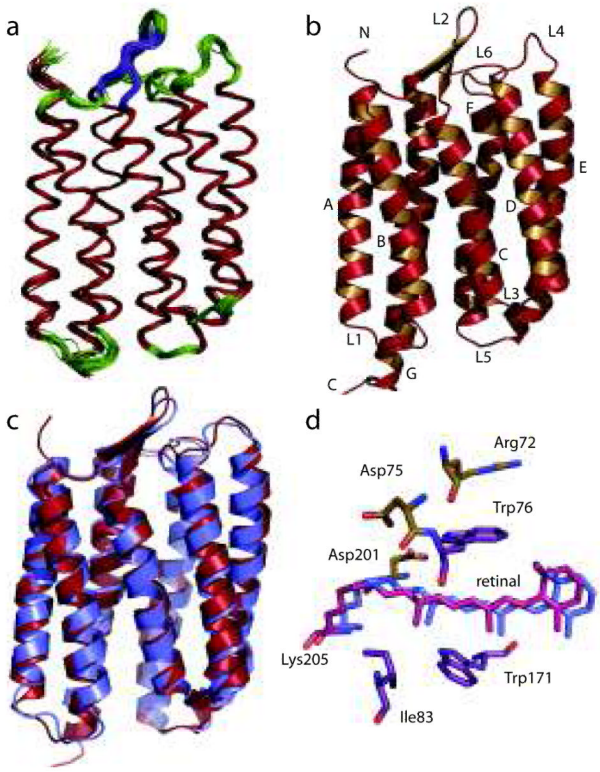

Figure 2.

Solution-NMR structure of pSRII in DHPC micelles. **(a)** An ensemble of 30 low-energy structures derived from NMR restraints. The backbone r.m.s. deviation for residues 1–221 is 0.48 Å. Loop and strand regions are indicated in green and purple, respectively. The 20 unstructured C-terminal residues are omitted from this figure. **(b)** Ribbon diagram of the structure closest to the mean. **(c)** Superposition of the NMR structure shown in **b** in red and the X-ray crystal structure 1H6823 in blue. The r.m.s. deviation of the best backbone superposition of the two structures for residues 1–219 is 1.23 Å. **(d)** All-*trans* retinal binding pocket viewed side-on showing the chromophore attached via a Schiff base to Lys205. The closest to the mean NMR structure is shown in pink superimposed on the X-ray structure displayed in blue. Selected side chains of residues contacting the retinal are shown for the NMR structure in purple. The two potential counter ions to the Schiff base Asp75 and Asp201 as well as Arg72 are displayed in brown.

Europe PMC Funders Author Manuscripts

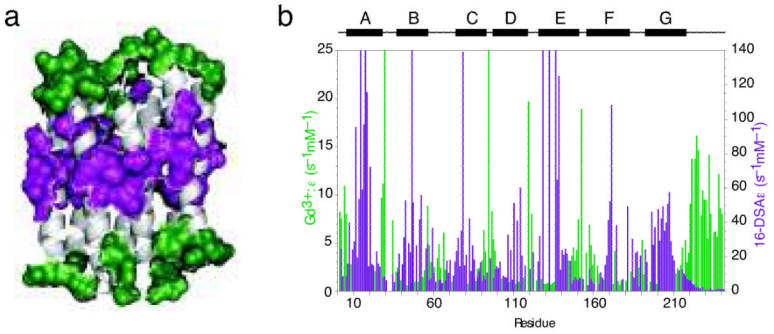

Figure 3.

Mapping of hydrophobic and solvent exposed regions of pSRII through titration with the detergent spin labels 16-DSA and gadoteridol. **(a)** Residues that experience a significant relaxation enhancement mapped onto the NMR structure of pSRII. Residues that interact with 16-DSA with a relaxation enhancement $\varepsilon > 35\ mM^{-1}s^{-1}$ are shown in purple. They are in close contact to the hydrophobic interior of the micelle. Solvent exposed residues that interact with the water-soluble gadoteridol resulting in an enhancement $\varepsilon > 4\ mM^{-1}s^{-1}$ are shown in green. These residues are in the vicinity of the polar detergent head groups possibly in contact with water. Residues represented in light grey are unaffected, with ε values below these thresholds. **(b)** Relaxation enhancement values obtained from the titration with the two spin labels. The same color scheme is employed as in **a**. A graphical representation of the secondary structure is displayed at the top of the diagram.

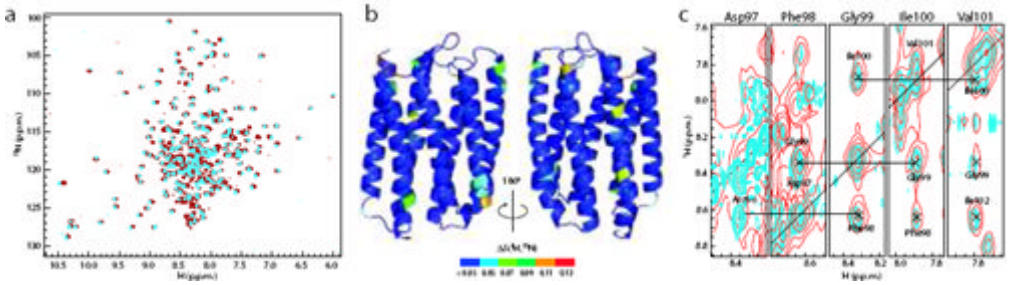

Figure 4.

Comparison of small bicelle versus micelle reconstitution of pSRII. **(a)** Overlay of [^{1}H,^{15}N]-TROSY correlation 2D spectra showing the backbone amide resonances of pSRII in DHPC micelles (cyan) and DMPC/c6-DHPC (q=0.3) small bicelles (red). **(b)** Chemical shift changes $\Delta\delta(^{1}H,^{15}N) = [(\Delta\delta^{1}H)^{2} + (\Delta\delta\ ^{15}N)^{2}/6]^{0.5}$ in **a** are mapped onto the structure of pSRII. Increasingly larger differences are indicated by a gradual color change from blue to red as shown in the figure. The differences between micelle and small bicelle environments are generally small. Affected residues are located on the exterior of the protein mainly towards the helix extremities. **(c)** Overlay of ^{1}H-^{1}H cross-sections from 3D ^{15}N-separated NOESY-HSQC spectra taken at the ^{15}N frequencies of residues 97–101 for pSRII solubilized in either a micelle (blue) or small-bicelle (red) environment. Despite the chemical shift changes observed for these residues, the cross-peak pattern is unchanged indicating the preservation of the structural features. Sequential NOEs are annotated. The larger line width in the small bicelle spectra is due to the slower tumbling of the protein–bicelle complex.

Europe PMC Funders Author Manuscripts

Table 1
NMR and refinement statistics for pSRII structures

	pSRII
NMR distance and dihedral constraints	
Distance constraints	
Total NOE	5564
Intra-residue	1561
Inter-residue	
Sequential ($\|i-j\| = 1$)	1336
Medium-range ($\|i-j\| < 4$)	1131
Long-range ($\|i-j\| > 5$)	1536
Hydrogen bonds	132
Total dihedral angle restraints	
φ (TALOS)	190
Ψ (TALOS)	190
Structure statistics	
Violations (mean ± s.d.)	
Distance constraints (Å)	0.0125 ± 0.0009
Dihedral angle constraints (°)	0.432 ± 0.044
Max. dihedral angle violation (°)	0.580
Max. distance constraint violation (Å)	0.0148
Deviations from idealized geometry	
Bond lengths (Å)	0.00173 ± 0.00006
Bond angles (°)	0.343 ± 0.007
Impropers (°)	0.263 ± 0.01
Average pairwise r.m.s. deviation[a] (Å)	
Heavy[b]	0.866
Backbone[b]	0.481

[a] Pairwise r.m.s. deviation was calculated among 30 refined structures.

[b] Statistics applied in transmembrane and loop regions (residues 1–221).